Asphaltene Diffusion and Adsorption in Modified NiMo Alumina Catalysts Followed by Ultraviolet (UV) Spectroscopy

ARTICLE *in* ENERGY & FUELS · JULY 2010

Impact Factor: 2.79 · DOI: 10.1021/ef1000979

4 AUTHORS, INCLUDING:

Melaz Tayakout-fayolle
Claude Bernard University Lyon 1
74 PUBLICATIONS **440** CITATIONS

SEE PROFILE

Denis Uzio
IFP Energies nouvelles
66 PUBLICATIONS **873** CITATIONS

SEE PROFILE

Energy Fuels **XXXX,** *XXX,* 000–000 · DOI:10.1021/ef1000979

energy&fuels
article

Asphaltene Diffusion and Adsorption in Modified NiMo Alumina Catalysts Followed by Ultraviolet (UV) Spectroscopy

Charles Marchal,*[,†] Eswar Abdessalem,[†] Melaz Tayakout-Fayolle,[‡] and Denis Uzio[†]

[†]*IFP-Lyon, Rond-point de l'échangeur de Solaize, BP 3, 69360 Solaize, France, and* [‡]*Université Claude Bernard Lyon 1, bât 308G ESCPE-Lyon, 2ème étage, 43 boulevard du 11 Novembre 1918, 69622 Villeurbanne Cedex, France*

Received January 27, 2010. Revised Manuscript Received June 18, 2010

Hindered diffusion and adsorption phenomena of asphaltene molecules inside the porous network of hydrotreatement catalysts are discussed in this paper. The kinetics of the global process was followed by visible absorption spectroscopy measurements. After *n*-heptane extraction, asphaltenes were dissolved in toluene at low concentration and put in contact with a given amount of catalyst. The dynamic of the diffusion−adsorption process was investigated by measuring the absorbance of monochromatic visible radiation (750 nm) versus contact time. The effects of the composition of the catalysts (alumina-supported NiMo with or without dopants, such as sodium and tin) have been investigated. Coke formation and asphaltene conversion have also been studied during the hydroconversion catalytic test. A modeling approach based on the "Stefan−Maxwell" formalism was applied, which takes into account the volume constraints by Fornasiero's formulation and assumes that the molecules collide only by an equivalent volume. The different parameter estimations have been performed and discussed to identify the controlling step of the process: mass transfer or asphaltene adsorption on the surface. The results show that dopants have only a moderate effect, with sodium addition decreasing the asphaltene adsorption constant, whereas it is slightly increased by tin. On the other hand, the coke deposit has a dramatic impact on the overall process, decreasing the effective diffusion coefficient as well as the adsorption constant of asphaltene. Moreover, after deep hydroconversion, the size of the asphaltene molecules is strongly decreased, the adsorption coefficient is enhanced, and diffusional coefficients increased by 1 order of magnitude.

Introduction

The decline of available oil resources coupled with the increase of the fuel demand compel refiners to process increasing volumes of heavy crudes. Middle distillate valuable fractions can be recovered converting atmospheric and vacuum residues in different thermal and/or catalytic processes based on carbon rejection or hydrogen addition schemes.[1] Among the major issues while upgrading residues, asphaltene handling is still an unsolved challenge mainly because of their high ability to flocculate and precipitate, contributing to the formation of deposits on the catalysts and equipment. Fouling results in the frequent shutdown of units and strongly decreases the efficiency of the process. It is then of main interest to improve the performances of hydrotreating catalysts to achieve longer cycle lengths.[2]

Asphaltenes have been extensively studied in the literature and are defined by a solubility class of molecules, insoluble in *n*-paraffins/soluble in toluene, with a very high molecular weight. They are made of polar aromatic compounds with mainly carbon (ca. 80−86 wt %), hydrogen (6−8 wt %), oxygen (0.5−2 wt %), nitrogen (0.5−2 wt %), sulfur (2−9 wt %), and metals (Ni and V associated with porphyrin structures).[3,4] Asphaltenes are characterized by broad size and molecular pattern distributions.

Models have been developed to provide a better molecular representation of asphaltenes, for instance, with the so-called continental or archipelago configurations.[5,6] The size of these structures ranges in a wide window from 10 to several hundreds of angstroms.[7] For instance, with small-angle neutron scattering (SANS), the radius of asphaltene structures was determined to be in the range of 30−100 Å, with a disk-like shape by Ravey et al.,[8] and Herzog et al. proposed a radius between 13 and 800 Å from small-angle X-ray scattering (SAXS) measurements.[9]

A high level of conversion of asphaltenes can be achieved under severe operating conditions of temperature and hydrogen pressure using heterogeneous catalysts. Dedicated technologies, such as an ebullated bed, have been developed to process high-metal-containing feedstocks.[10,11] Catalyst characteristics are also important to improve the performances, and textural properties of the support have been found to be a

*To whom correspondence should be addressed. Telephone: +33478022020. E-mail: charles.marchal@ifp.fr.

(1) Rana, M. S.; Samano, V.; Ancheyta, J.; Diaz, J. A. I. *Fuel* **2007**, *86*, 1216–1231.
(2) Gawel, I.; Bociarska, D.; Biskupski, P. *Appl. Catal., A* **2005**, *295*, 89–94.
(3) Speight, J. G. The realms and definitions of asphaltenes. In *Constituents and Asphalts. Developments in Petroleum Science*; Elsevier: Amsterdam, The Netherlands, 1994; pp 7−28.
(4) Abu-Khader, M.; Speight, J. G. *Oil Gas Sci. Technol.* **2007**, *62*, 715–722.
(5) McCaffrey, W. C.; Sheremata, J. M.; Gray, M. R.; Dettman, H. *Proceedings of the 4th International Conference on Petroleum Phase Behavior and Fouling*; Trondheim, Norway, June 23−26, 2003.
(6) Murgich, J. *Mol. Simul.* **2003**, *29*, 451–461.
(7) Baltus, R. E.; Anderson, J. L. *Chem. Eng. Sci.* **1983**, *38*, 1959–1969.
(8) Ravey, J. C.; Ducouret, G.; Espinat, D. *Fuel* **1988**, *67*, 1560–1567.
(9) Herzog, P.; Tchoubar, D.; Espinat, D. *Fuel* **1988**, *67*, 245–250.
(10) Morel, F.; Kressmann, S.; Harlé, V.; Kasztelan, S. In *Hydrotreatment and Hydrocracking of Oil Fractions*; Froment, G. F., Delmon, B., Grange, P., Eds.; Elsevier: Amsterdam, The Netherlands, 1997; Studies in Surface Science and Catalysis, Vol. 106.
(11) Duddy, J. E.; Wisdom, L. I.; Kressmann, S.; Gauthier, T. *Proceeding of the 3rd Bottom of the Barrel Technology Conference and Exhibition*; Antwerp, Belgium, Oct 20−21, 2004.

critical parameter. Pore size distribution including a mixture of large macropores and smaller mesopores seems to be a compromise to combine suitable diffusion properties and sufficient surface area, giving access to a large number of active sites.[12]

Many studies were focused on asphaltene characterization and phenomenon governing aggregation in different medium,[13,14] but still more investigations are required to have a better understanding of the diffusion and adsorption process in the porous network of hydrotreating catalysts. Asphaltenes are known to exhibit a high tendency to adsorb on the catalyst surface, blocking the entrance of the pores, and further on the access to active sites. Asphaltenes are supposed to interact with acidic sites through basic nitrogen.[15,16] In the case of VO−porphyrins extracted from Boscan crude, Galiasso and Morales[17] reported that diffusion is strongly influenced by surface acidity and particle size; large particles and acidic surfaces exhibited the lowest diffusion rates and metal porphyrin adsorption capacity. Morales et al.[18] proposed an interaction through the oxygen ligand of the vanadyl group with the electron acceptor (Lewis acid sites) of the γ-Al_2O_3 surface. On the other hand, on a sulfided CoMo-supported catalyst, the interaction is likely to take place via a transfer from an electron-donor site (basic Lewis or Brönsted surface site, such as O^{2-} or OH^-) to the vanadyl group. Knözinger et al.[19] proposed that adsorption sites on both alumina and sulfided Mo/Al_2O_3 catalyst are located on an uncovered support surface and proceed via two forms of donor−acceptor interactions. Among the studies dedicated on diffusion of asphaltenes in porous solids, Xiaofeng et al.[20] using a diffusion−adsorption model showed that, when increasing the molecular weight of the asphaltene fraction, the adsorption constant monotonically increases and the effective diffusivity decreases. Liu et al.[21] focused on the diffusion of various vacuum residua fractions in a 23 nm SiO_2 model catalyst and concluded that the diffusion coefficient decreases with the average molecular weight of the oil fraction from 4.6×10^{-10} to 0.5×10^{-10} m^2/s. Interesting results from Mieville et al.[22] also highlight the strong influence of macroporosity on the diffusion coefficient and the hindering effect of the coke deposit on diffusion of asphaltenes. Östlund et al.[23] using pulsed field gradient spin echo nuclear magnetic resonance (PGF−SE NMR) concluded a disk-like-shaped asphaltene model from a Venezuelan crude oil with a diffusion coefficient at infinite dilution of 2.2×10^{-10} m^2/s.

Collins and Melrose found that the presence of water, either pre-adsorbed on the mineral surface or co-adsorbed with the asphaltenes, decreases the amount of asphaltene adsorption on the clay. As a general rule, the presence of water decreases but does not fully hinder the adsorption of asphaltenes.[24] In the present study, we will see that the maximum of pre-adsorbed water on our solids is far below the values supposed to interfere with asphaltene adsorption.[25]

More recently, several studies have brought new insight into the comprehension of changes in the chemical nature of asphaltene during hydroprocessing.[2,26] Using size-exclusion chromatography and ^{13}C NMR, it has been shown that aromaticity of unconverted asphaltenes increases with the conversion level mainly because of dealkylation reactions. In a comprehensive study on chemical changes during hydrotreatment, Bartholdy et al. report that the temperature transition between the catalytic hydrogenation reaction and high-temperature thermal cracking regime is in the range of 370−390 °C and feed-dependent. Sludge formation is a result of the precipitation of small residual asphaltenes, and the whole oil, including the stabilizing fraction (resins), is chemically modified.[27] Gonzalez et al.[28] showed that, in the case of archipelago-type asphaltenes, the hydrocarbon skeleton plays a minor role upon adsorption compared to the nature and content of the heteroatom. Oxygen and, particularly, nitrogen present in the structure of the adsorbed molecules were found to be the heteroatoms determining the adsorption dynamics over macroporous kaolin.

In the present study, ultraviolet (UV) spectroscopy has been used to investigate the effect of surface acidobasic properties of modified $NiMo/\gamma$-Al_2O_3 catalysts on diffusion and adsorption properties of fresh and residual Safaniya asphaltenes recovered after the hydrotreating catalytic test performed at different conversion levels. Using a recently developed model,[29] different parameters, such as effective diffusivity or adsorption coefficients, have been determined to assess the respective contributions of the diffusion process of the species in the porous network and the adsorption step via the interactions with the acid−base surface sites.

Table 1. Main Characteristics of SVR

Ni (ppm)	43
V (ppm)	143
S (wt %)	4.8
N (wt %)	0.37
C (wt %)	84.6
H (wt %)	10.1
specific gravity	1.0277
viscosity at 100 °C (cSt)	1516
C7 asphaltenes (wt %)	11.9
conradson carbon (wt %)	20

Experimental Section

Asphaltene Preparation. In the present work, asphaltenes have been recovered in hot *n*-heptane using the Association Française de Normalisation (AFNOR) T60-115 method. Unconverted asphaltenes (Asph0) have been extracted from a Safaniya vacuum residue (SVR). The main properties of the SVR feedstock are reported in Table 1. Converted asphaltenes

(12) Ancheyta-Juarez, J.; Maity, S. K.; Betancourt-Rivera, G.; Centeno-Nolasco, G.; Rayo-Mayoral, P.; Gomez-Pérez, M. *Appl. Catal., A* **2001**, *216*, 195–208.
(13) Espinat, D.; Rosenberg, E.; Scarsella, M.; Barre, L.; Fenistein, D.; Broseta, D. In *Structures and Dynamics of Asphaltenes*; Mullins, O. C., Sheu, E. Y., Eds.; Plenum Press: New York, 1998.
(14) Merdrignac, I.; Espinat, D. *Oil Gas Sci. Technol.* **2007**, *62*, 7–32.
(15) Speight, J. G. In *Asphaltenes and Asphalts*; Yen, T. F., Chilingarian, G. V., Eds.; Elsevier: Amsterdam, The Netherlands, 1994; Vol. 1, p 60.
(16) Melo Faus, F.; Grange, P.; Delmon, B. *Appl. Catal.* **1984**, *11*, 281–293.
(17) Galiasso, R.; Morales, A. *Appl. Catal.* **1983**, *7*, 57–74.
(18) Morales, A.; Marrero, C.; Galiasso, R. *Proceeding of the 8th International Congress on Catalysis*; Berlin, Germany, 1984; Vol. *2*, p 341.
(19) Knözinger, H.; Cordischi, D.; Vielhaber, B. *Catal. Today* **1990**, *7*, 447–466.
(20) Yang, X.; Guin, J. A. *Chem. Eng. Commun.* **1998**, *166*, 57–79.
(21) Liu, Z.; Chen, S. L.; Dong, P.; Gao, J.; Ge, X.; Xu, Z. *Energy Fuels* **2009**, *23*, 2862–2866.
(22) Mieville, R. L.; Trauth, D. M.; Robinson, K. K. *Prepr.—Am. Chem. Soc., Div. Pet. Chem.* **1989**, *34*, 635.
(23) Östlund, J. A.; Andersson, S. I.; Nydén, M. *Fuel* **2001**, *80*, 1529–1533.
(24) Collins, S. H.; Merose, J. C. *Proceeding of the Society of Petroleum Engineers* (*SPE*) *International Symposium on Oilfield and Geothermal Chemistry*, Denver, CO, 1983.
(25) Menon, V. B.; Wasan, D. T. *Colloids Surf.* **1986**, *19*, 107–122.
(26) Gauthier, T.; Danial-Fortain, P.; Merdrignac, I.; Guibard, I.; Quoineaud, A. A. *Catal. Today* **2008**, *130*, 429–438.
(27) Bartholdy, J.; Lauridsen, R.; Mejlholm, M.; Andersen, S. I. *Energy Fuels* **2001**, *15*, 1059–1062.
(28) Gonzalez, M. F.; Stull, C. S.; Lopez-Linares, F.; Pereira-Almao, P. *Energy Fuels* **2007**, *21*, 234–241.
(29) Tayakout, M.; Ferreira, C.; Espinat, D.; Arribas Picon, S.; Sorbier, L.; Guillaume, D.; Guibard, I. *Chem. Eng. Sci.* **2009**, *65* (5), 1571–1583.

Table 2. Extra- and Intragranular Porosities and Pore Radii of the Catalysts and Initialization Condition

	NiMo	Na−NiMo	Sn−NiMo	spent NiMo
wt % dopant		0.27	0.33	
density, ρ_{cata} (kg/m^3)	1009	1011	1025	1399
mesoporous volume, $V_{meso\ (70-500)}$ (mL/g)	0.20	0.20	0.21	0.07
intragranular porosity, ε_p[a]	0.202	0.202	0.215	0.101
extragranular porosity, ε_i[b]	0.935	0.935	0.936	0.953
mean pore diameter, d_0[c] (Å)	250	250	248	260
coke (wt %)	0	0	0	19.5
specific surface area (BET) (m^2/g)	305	306	308	146

[a] Calculated using eq 20. [b] Calculated using eq 21. [c] Calculated using eq 22.

have been obtained by hydroconversion catalytic tests of the SVR performed in a 300 mL stainless-steel batch reactor under constant pressure in the presence of 15 mL of presulfided NiMo/γ-Al_2O_3 catalyst and 90 mL of SVR. The operating conditions were the following: temperature, 430 °C; constant pressure, 14.5 MPa; catalyst/oil weight ratio, 0.1; stirring rate, 900 rpm. The reaction time has been adjusted to obtain different asphaltene conversion levels. After 1 h and 12 min of reaction, the conversion of asphaltenes reaches 80%; these asphaltenes will be designated as Asph80. For a reaction time of 2 h, the asphaltene conversion level reaches 90% (Asph90). Asphaltene density is measured by a Minidens solid densimeter. The asphaltenes are dissolved in toluene (Carl-Erba, 99.8% purity). To avoid the formation of large unstable aggregates usually observed at high concentration (0.25 wt % is the onset of "macro" aggregation found in ref 30), asphaltene concentration in toluene is fixed at 0.15 wt %, so that asphaltenes can be seen as stable "nano" aggregates.

Catalyst Characteristics. The physicochemical characteristics of the different catalyst samples are presented in Table 2. Starting from a standard NiMo/γ-Al_2O_3 hydrotreating catalyst with a meso−macro bimodal pore size distribution, a 0.9 mm diameter cylindrical extrudate shape, and a length of 3 mm, different additives (Na and Sn) have been used to modify the acidobasic surface properties of this starting material. After incipient wetness impregnation of precursors, $Sn(C_4H_9)_4$ in *n*-heptane and $NaNO_3$ in water, samples were maturated for 24 h at room temperature in a water-controlled humidity cell, dried for 24 h at 120 °C, and calcined for 2 h at 500 °C under air flow. Using a JEOL JXA 8100 electron-probe microanalyzer, it has been checked that the different additives were uniformely dispersed across the diameter of the extrudates. Tin and sodium amounts in the catalyst have been determined by inductively coupled plasma−atomic emission spectroscopy (ICP−AES). Used catalyst is obtained after SVR hydroconversion catalytic tests as previously described. The spent catalyst is recovered and washed 3 times with toluene in a reflux system (Soxtherm, Gerhardt, Germany) at the boiling point of the solvent (110 °C at atmospheric pressure) for 7 h to remove the soft part of coke. The solid is then dried in an oven at 150 °C for 3 h. Coke is defined in this work as the carbon content of the spent catalyst after washing by hot toluene. The specific surface area and mesopore size distribution have been determined from N_2 isotherms at 77 K using a Micromeritics ASAP2420 apparatus after heating at 350 °C for 4 h (300 °C for the coked catalyst). Hg porosimetry has also been used to obtain the whole pore size distribution, including the macroporosity, and performed on a Micromeritics Autopore IV 9500 series porosimeter after a thermal treatment at 250 °C for 4 h. Finally, optic microscopy has been performed using an Olympus BX51 microscope.

UV Spectrometry. Asphaltene aggregate diffusion versus time was followed using a UV−vis spectrometer, Cary 4G (Varian). The catalyst is weighed and previously mixed with the toluene, so that the whole porosity of the solid is filled by the solvent. The excess of toluene is then removed. A 10 mm quartz cell (Hellma-QS) is filled with 0.25 g of catalyst and 2.5 g of a solution containing 0.15 wt % asphaltene in toluene. The asphaltene/catalyst weight ratio is close to 1.5. Experiments were performed at a constant room temperature of 24 °C.

A large space in the cell, free of material, allows for the correct absorption measurement of a monochromatic radiation (750 nm) (I/I_o). The cell temperature and radiation intensity (I_0) fluctuations are corrected by a comparison to the reference cell (I_{ref}/I_o) filled with pure toluene. The measured ratio (I/I_{ref}) can be recorded as a function of time. The absorbance $A = -\log(I_{ref}/I)$ depends upon the asphaltene concentration in the solution according to the following expression (Beer−Lambert's law):

$$A = \varepsilon l c \quad (1)$$

where l is the cell thickness (cm), c is the asphaltene concentration (mol/L), and ε is the molar absorption coefficient (L mol^{-1} cm^{-1}), which is characteristic of the interaction between incident radiation and asphaltene molecules. In the figures presented in this paper, the relative concentration (C/C_0) is plotted versus time.

It has been checked that the variation of the intensity with the amount of asphaltene in toluene was perfectly linear (below 0.25 wt %) for both unconverted and converted asphaltenes in a diluted range, chosen to limit aggregation phenomenon as mentioned in the asphaltene preparation section (Figure 4). The linearity of the calibration plot means that the "nano" aggregates do not affect the behavior of the chromophores. Moreover, stability of the intensity versus time without catalyst confirmed the absence of large aggregation and showed that no significant evaporation of the solvent took place during the experimental interval. Repeating the same adsorption/diffusion experiment (unconverted asphaltenes, NiMo catalyst) 4 times allowed for the determination of the measurement accuracy of ±0.015 (Asph0, NiMo catalyst) and is supposed to be the same for each experiment.

Mathematical Model. In this section, a brief description of the mathematical model is given. A more detailed description is reported elsewhere.[29] The model assumes that the contact between alumina and asphaltene solution takes place in a tank at constant volume and temperature conditions. The model is based on the "Stefan−Maxwell" equations taking into account the volume constraints defined by Fornasiero et al.,[31−33] which suggest that collisions between solvent molecules and the solute involve a small part of the largest molecule (asphaltene). The size of this collision area is not very different from the size of the solvent molecule. Thus, the solute molecule can be represented by several connected beads or segments ($n_{s,asph}$), each having the same frictional properties.

This model considers the following assumptions: (i) The liquid mixture is ideal. (ii) The molar volumes in the liquid and adsorbed phases are identical. (iii) The adsorption equilibrium is represented by the generalized Langmuir model, and the local equilibrium hypothesis is assumed along the whole radius. (iv) Studied catalysts are cylindrical extrudates with a diameter of 0.9 mm and an average length of 3 mm. (v) The catalyst support has a meso−macro

(30) Durand, E.; Clemancey, M.; Lancelin, J. M.; Verstraete, J.; Espinat, D.; Quoineaud, A. A. *J. Phys. Chem. C* **2009**, *113*, 16266–16276.

(31) Fornasiero, F.; Prausnitz, J. M.; Radke, C. J. *Macromolecules* **2005**, *38*, 1364–1370.

(32) Hassou, M.; Couenne, F.; Le Gorrec, Y.; Tayakout, M. *AIChE J.* **2009**, *55*, 2094–2105.

(33) Ferreira, C.; Marques, J.; Tayakout, M.; Guibard, I.; Lemos, F.; Toulhoat, H.; Ramôa Ribeiro, F. *Chem. Eng. Sci.* **2010**, *65* (1), 322–329.

bimodal pore size distribution. We assume that only the mesopore range contributes to the mass-transfer resistance. (vi) The mass transfer in the catalyst support takes place in the radial position and is described by the Maxwell−Stefan equation, taking into account the volume constraints. (vii) Mass-transfer resistance at the pellet surface is lumped into a single external film mass-transfer coefficient, k_{asph}. (viii) Intragranular porosity and pore diameter variations are taken into account via the adsorbed volume. (ix) The catalyst is supposed to be filled by the solvent before the beginning of asphaltene diffusion.

Material Balances. The previous hypotheses lead to the following set of equations (see the Nomenclature). In these equations, the subscript "asph" stands for asphaltene molecules and the subscript "tol" stands for toluene used as a solvent for asphaltene solutions. The superscripts "f" and "p" refer to the fluid or porous (catalyst) phases, respectively. The mass balances are established in volume fraction, taking into account that the concentration is defined as follows: $C_i^j = (\phi_i^j/n_{s,i}\vartheta^0)$, with $n_{s,i}$ being the segment number ($n_{s,tol} = 1$) and $\vartheta^0 = \vartheta_{tol}$.

Considering a cylindrical pellet, the mass balance in the bulk fluid of the quartz cell, expressed in fluid volume fractions, is given by eq 2.

$$\frac{\partial \phi_{asph}^{f}}{\partial t} = \frac{(1-\varepsilon_i)}{\varepsilon_i}\frac{2}{R_p}k_{asph}(\phi_{asph}^{f} - \phi_{asph}^{p}(R_p,t)) \quad (2)$$

$$\text{and } \phi_{tol}^{f} = 1 - \phi_{asph}^{f} \quad (3)$$

The mass balance in the mesoporosity of a cylindrical pellet written in fluid volume fractions is given by eq 4.

$$\varepsilon_p\frac{\partial \phi_{asp}^{p}(r,t)}{\partial t} + n_{s,\,asph}\vartheta_{tol}(1-\varepsilon_p)\frac{\partial q_{asp}(r,t)}{\partial t} = n_{s,\,asph}\vartheta_{tol}\varepsilon_p\frac{1}{r}\frac{\partial}{\partial r}(rN_{asp}(r,t)) \quad (4)$$

The flux described with the number of segments is given by $N_{asp}^0 = n_{s,asph}N_{asph} = (D_{eff}/n_{s,asph}\vartheta_{tol})\nabla\phi_{asp}^{p}$. The adsorption equilibrium is represented by the generalized Langmuir model, $q_i = (q^{max}b_iC_i^p/(1 + \sum_{j=1}^{nc} b_jC_j^p))$

When the two above equations are substituted into eq 4, the mass balance in the mesoporosity of a cylindrical pellet could be written as in eq 5.

$$\left(\varepsilon_p + \frac{(1-\varepsilon_p)q^{max}b_{asph}}{(1+\sum_{j=1}^{nc} b_jC_j^p)^2}\left((1+b_{tol}C_{tol}^p) + \frac{n_{s,\,asph}}{n_{s,\,tol}}b_{tol}C_{asph}^p\right)\right)\frac{\partial \phi_{asph}^{p}(r,t)}{\partial t} = \frac{D_{eff}}{n_{s,\,asph}}\frac{1}{r}\frac{\partial}{\partial r}\left(r\frac{\partial \phi_{asph}^{p}}{\partial r}\right) \quad (5)$$

The boundary conditions are

$$\forall t \quad \text{at} \quad r = r_p \quad \frac{D_{eff}}{\varepsilon_p n_{s,\,asph}}\left.\frac{\partial \phi_{asp}^{p}}{\partial r}\right|_{r=R_p} = k_{asph}(\phi_{asph}^{f} - \phi_{asph}^{p}(R_p,t))$$
$$\forall t \quad \text{at} \quad r = 0 \quad \left.\frac{\partial \phi_{asph}^{p}}{\partial r}\right|_{r=0} = 0 \quad (6)$$

Porosity and pore radius variations have been calculated using the method of Tayakout et al.,[29] as shown in eq 7.

$$\frac{\varepsilon_p(r,t)}{\varepsilon_p(r,0)} = \frac{V(r,t)}{V(r,0)} \quad (7)$$

If we consider a cylindrical model of porous geometry with a pore length, L, and radius, r, the last relation can be written as

$$r_0(r,t) = r_0(r,0)\sqrt{\frac{\varepsilon_p(r,t)}{\varepsilon_p(r,0)}} \quad (8)$$

To obtain the pore radius, the intragranular porosity at a given time is calculated through a volume balance as shown in eq 9.

$$\varepsilon_p(r,t) = \frac{\varepsilon_p(r,0) - q_{asp}(r,t)\vartheta_{tol}n_{s,\,asp} - q_{tol}(r,t)\vartheta_{tol}n_{s,\,tol}}{1 - q_{asp}(r,t)\vartheta_{tol}n_{s,\,asp} - q_{tol}(r,t)\vartheta_{tol}n_{s,\,tol}} \quad (9)$$

$$\text{with } q_i = \frac{q^{max}b_iC_i^p}{1+\sum_{j=1}^{nc} b_jC_j^p} \quad i = 1, nc \quad (10)$$

Model Initialization. The experimental initial conditions considered in the model are the following:

$$t = 0 \quad \text{fluid phase} \quad \begin{vmatrix} W_{asph}^{f}(t=0) = W_{asph}^{0,f} \\ W_{tol}^{f}(t=0) = W_{tol}^{0,f} \end{vmatrix} \quad (11)$$

$$t = 0 \quad \text{porous phase} \quad \begin{vmatrix} W_{asph}^{p} = 0 \\ W_{tol}^{p} = 1 \end{vmatrix} \quad (12)$$

As the experimental results are acquired in mass fractions and the model is written in volume fractions, an experimental data treatment was needed to obtain the model feed

$$\phi_i^p = \frac{\rho_T n_{s,\,i}\vartheta_{tol}}{M_i}W_i^p \quad i = 1, nc \quad (13)$$

Estimated Parameters. Five parameters are estimated by fitting the model to the experimental data: (1) the translational diffusion coefficient (D_∞), (2 and 3) the thermodynamical parameters governing the adsorption of toluene and asphaltene aggregate (b_{asph} and b_{tol}), (4) the saturation concentration (q^{max}), and (5) the asphaltene aggregate segment number ($n_{s,asph}$).

The translational phase diffusion coefficient, D_∞, and number of segments, $n_{s,asph}$, are estimated for each asphaltene conversion level (Asph0, Asph80, and Asph90) and kept constant for all other estimations. When the catalyst used for the experiment does not change, the thermodynamic Langmuir coefficient of toluene (b_{asph}) and the saturation concentration (q^{max}) are kept constant.

Calculated Parameters. *Effective Diffusion Coefficient*. Concerning the effective diffusion coefficient, a mathematical hydrodynamic model has been proposed for hindered diffusion[34,35] and allows its calculation from the translational diffusion coefficient (D_∞).

Two main phenomena are taken into account:

The first one is a partitioning of the solute $\left(K_p = \frac{\phi_{asph}^{p}}{\phi_{asph}^{f}}\right)$ (14)

The second one, because of the pore wall, is an increased viscous drag on a solute molecule as it tries to move through the solvent within the pore, so that the molecule mobility is reduced.

Two expressions for K_p and K_r have been proposed in the literature,[34] depending upon the ratio $\lambda = R_h/r_o$, where R_h is the hydrodynamic radius of asphaltene nano-aggregates considered spherical and r_0 is the average pore radius.

$$K_p = (1-\lambda) \quad (15)$$

$$K_r = 1 - 2.104\lambda + 2.089\lambda^3 - 0.948\lambda^5 \quad (16)$$

Taking both effects into account, the effective diffusion coefficient can be calculated using the following expression (eq 17), which is accurate for $\lambda \leq 0.5$:

$$D_{eff} = \varepsilon_p K_r K_p D_\infty \quad (17)$$

where ε_p is the intragranular porosity.

Considering a spherical morphology of asphaltene nano-aggregates, the hydrodynamic diameter D_h can be calculated

(34) Deen, W. M. *AIChE J.* **1987**, *33*, 1409–1425.
(35) Yang, X.; Guin, J. A. *Chem. Eng. Commun.* **1998**, *166*, 57–79.

Table 3. Properties of Toluene and Asphaltene Aggregates (Initialization Condition)

toluene				asphaltenes	
density, ρ_{tol} (kg/m^3)	molecular weight, M_w (g/mol)	molar volume, ϑ_{tol} (m^3/mol)	viscosity, η_{tol} (Pa s)	density, ρ_{asph} (kg/m^3)	concentration (wt %)
867	92	1.061×10^{-4}	5.9×10^{-4}	1170	0.15

according to the Stokes−Einstein equation

$$D_h = \frac{2kT}{6\pi\eta D_\infty} \quad (18)$$

where η is the solvent viscosity and D_∞ the translational diffusion coefficient.

Molecular Weight. The molecular weight of asphaltene nano-aggregates is calculated according to eq 19

$$M_w = \rho_{asph}\vartheta_{tol}n_{s,asph} \quad (19)$$

where ρ_{asph} is the density of asphaltenes, ϑ_{tol} is the molar volume of toluene, and $n_{s,asph}$ is the number of segments of component i, relative to the elementary volume. The molar volume of asphaltene is given by $\vartheta_{asph} = n_{s,asph}\vartheta_{tol}$.

Intra- and Extragranular Porosities. Intra- and extragranular porosities have been assessed taking into account the following hypothesis: asphaltene nano-aggregates do not penetrate into pores with a diameter lower than their hydrodynamic diameter. The hydrodynamic diameter of Safaniya asphaltene aggregates has been estimated to be close to 66 Å.[29] As a consequence, intragranular porosity (ε_p) is defined in our study as the catalyst mesopores in the 70−500 Å range. The extragranular porosity (ε_i) is essentially the packed-bed porosity (void fraction between catalyst extrudates) plus the porosity of the macropores (pore size > 2000 Å). As shown in Figure 3, the volume of the pores between 500 and 2000 Å is negligible because the catalysts used in this work have a meso−macro bimodal pore size distribution. Diffusion resistance is supposed to occur only in intragranular porosity (ε_p). The mass-transfer resistance in macropores is not taken in consideration because D_{eff} is only reduced by 7% for a pore size equal to 2000 Å ($\lambda = 0.033$).

Hence, the intragranular porosity is calculated according to the following relationship:

$$\text{at } t = 0\ \forall r \quad \varepsilon_p = V_{meso}\rho_{cata} \quad (20)$$

where V_{meso} is the porous volume corresponding to mesopores (from 70 to 500 Å) per mass units, determined by Hg porosimetry (Figure 3).

On the other hand, the extragranular porosity is given by

$$\varepsilon_i = \frac{V_{liq} + V_{macro}}{V_{liq} + V_{cata}} = \frac{\left(\frac{m_{asph+tol}}{\rho_{asph+tol}}\right) + V_{macro}m_{cata}}{\left(\frac{m_{asph+tol}}{\rho_{asph+tol}}\right) + \frac{m_{cata}}{\rho_{cata}}} \quad (21)$$

where V_{liq} is the volume of the liquid asphaltene + toluene solution, V_{macro} is the volume of the macroporous catalyst network, V_{cata} is the volume of the catalyst, $m_{asph+tol}$ is the mass of the diluted asphaltene solution, $\rho_{asph+tol}$ is the density of the solution, m_{cata} is the mass of the catalyst, and ρ_{cata} is the specific mass of the catalyst grain.

The average pore diameter (d_o), representing pores at which hindered diffusion occurs, is calculated using Hg porosimetry measurements, as shown in eq 22

$$d_0 = \frac{\sum_{70}^{500} yx\mathrm{d}x}{\sum_{70}^{500} y\mathrm{d}x} \quad (22)$$

where x is the catalyst pore diameter and y is the injected Hg volume.

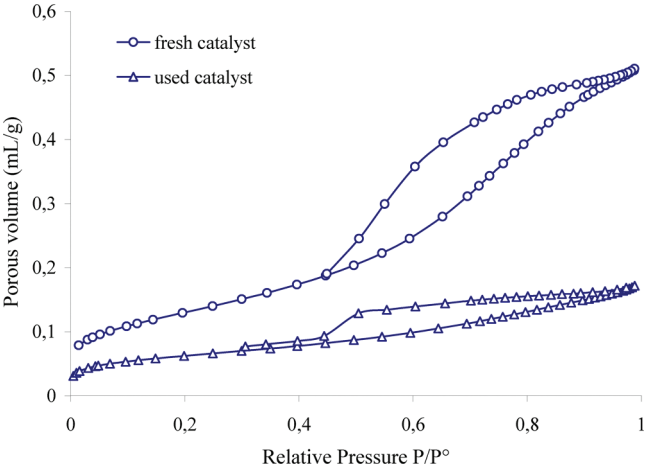

Figure 1. Nitrogen adsorption isotherm for fresh and spent NiMo catalysts.

Mass-Transfer Coefficient. In this work, the pellet is considered as a sphere equivalent. The mass-transfer coefficient of asphaltenes (k_{asph}) is obtained by solving the differential eq 23, which describes the concentration in the surrounding fluid as a function of the radius, for a sphere in an infinite fluid.[36]

$$\mathrm{Sh}_i = \frac{2R_p k_i^m}{D_{i,oil}} = 2 \quad (23)$$

Liquid Diffusion Coefficient. The liquid diffusion coefficient of asphaltene aggregates in toluene was calculated using the Scheibel correlation, as shown in eq 24[37]

$$D_{asp,tol}\ (\mathrm{cm}^2/\mathrm{s}) = 1 \times 10^{-8}\frac{T}{\eta_{tol}\vartheta_{asp}^{1/3}}\left(1 + \left(\frac{3\vartheta_{tol}}{\vartheta_{asp}}\right)^{2/3}\right) \quad (24)$$

where η_{tol} is the viscosity of toluene (in cP) and ϑ_{tol} and ϑ_{asp} are toluene and asphaltene molar volumes (mL/mol), respectively, with $\vartheta_{asp} = n_{asp}\vartheta^0$.

All data used to calculate parameters are given in Tables 2 and 3. T3

Numerical Method. The computing code based on the previous model has been developed in FORTRAN. Orthogonal collocations were used as a spatial discretization method. Subroutines JCOBI and DFOPR developed by Villadsen et al.[38] were used. The resulting ordinary differential algebraic system of equations is solved by the DDASPG integration sub-routine (IMSL library) based on the Petzold−Gear BDF method. The five parameters are grouped in the parameter vector (θ). The optimization is performed by a Levenberg−Marquard procedure (sub-routine DBCLSF of the IMSL library). The criterion to minimize with respect to θ is the sum of the square difference between the experimental and simulated results taking as a physical constraint that parameters are non-negative.

(36) Bird, F. B.; Stewart, W. E.; Lightfoot, E. N. *Transport Phenomena*; John Wiley and Sons: New York, 1960.
(37) Li, J.; Carr, P. W. *Anal. Chem.* **1997**, *69*, 2530–2536.
(38) Villadsen, J.; Michelsen, M. L. *Solution of Differential Equation Models by Polynomial Approximation*; Prentice Hall: Englewood Cliffs, NJ, 1978; p 446.

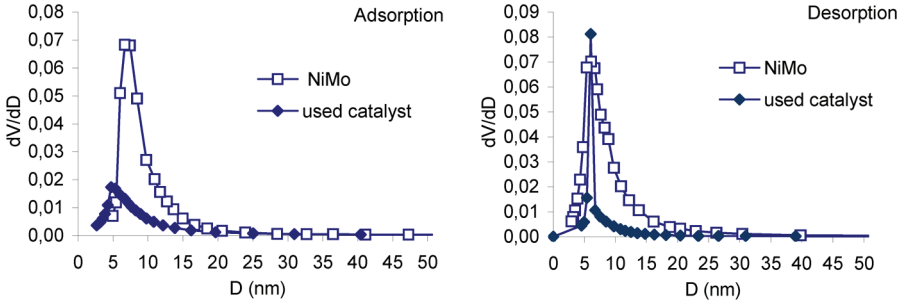

Figure 2. Pore size distributions obtained from nitrogen adsorption and desorption isotherms for fresh and used NiMo catalyst.

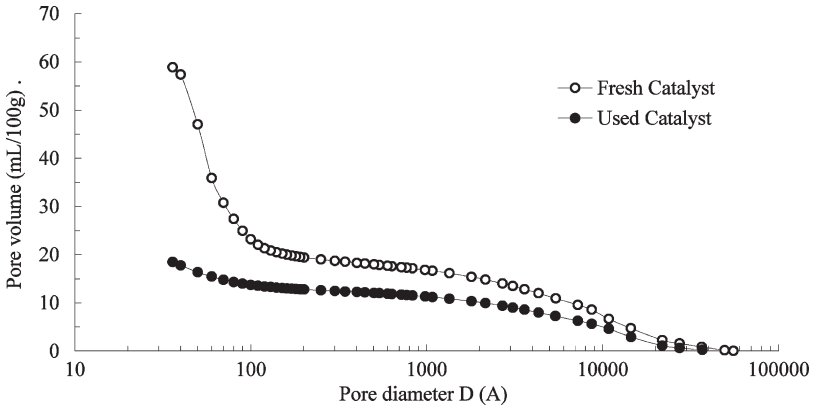

Figure 3. Bimodal pore size distribution of fresh and spent NiMo catalysts determined by Hg porosimetry.

The precision of estimated parameters is calculated using the following assumptions. First, errors associated with two successive measurements are independent and centered. They follow a normal distribution, of which the variance is estimated by $\sigma^2 = (1/(N_p - k)) \sum_{i=1}^{N_p} [\phi^f_{asp,meas}(i) - \phi^f_{asp,mod}(i)]^2$, where $\phi^f_{asp,mod}(i)$ and $\phi^f_{asp,meas}(i)$ are the calculated and measured outputs at the ith sample time, respectively, N_p is the number of sample points, and k is the number of parameters θ_j. Moreover, the precision of each parameter θ_j is calculated as follows: $\hat{\theta}_j - s_{N-k}(H_{jj}\sigma^2)^{1/2} < \theta_j < \hat{\theta}_j + s_{N-k}(H_{jj}\sigma^2)^{1/2}$, where $\hat{\theta}_j$ is the estimation of θ_j, H_{jj} is the jth diagonal element of the Hessian matrix H, and s_{N-k} is the student variable.[38−40]

The Hessian matrix $H = S^T S$ is calculated using the kN analytical sensitivity matrix S. The elements of S are defined as follows: $S_{ij} = (\partial\phi^f_{asp}(i)/\partial\theta_j)$. The S matrix is numerically calculated.

Results and Discussion

Figure 1 presents the nitrogen adsorption measurement for the fresh and spent catalysts after the residue hydroconversion catalytic test. Isotherms are classical type IV according to International Union of Pure and Applied Chemistry (IUPAC) classification, with a typical hysteresis loop for mesoporous materials. Specific surface area and porous volume are dramatically decreased by coke deposition, as shown in Table 2. Pore size distributions (Figure 2) obtained from adsorption and desorption isotherms, using a Barrett−Joyner−Halenda (BJH)-derived model,[41] are very similar for the fresh catalyst, whereas in the case of the coked catalyst, desorption abruptly occurs in a very narrow range of small pores (around 60 Å). Coke deposition modifies the network of the mesopores larger than 60 Å, which access the vapor phase only via these 60 Å windows.

Cumulative porous volume distributions for fresh and spent NiMo catalysts obtained from Hg porosimetry are presented in Figure 3. The results show a meso−macro bimodal pore size distribution for the two catalysts. Hg porosimetry measurements also showed a decrease of the total porous volume from 0.59 mL/100 g for the fresh catalyst to 0.19 mL/100 g for the spent one because of high coke loading (coke = 19.5 wt %) (Table 2). Finally, the two contributions are very distinct, and the porous volume between 500 and 2000 Å is very low, about 0.3 cm^3/g.

The adsorption−diffusion dynamic of the standard case (fresh catalyst and unconverted asphaltenes extracted from the feed) is shown in Figure 5. Calibration curves used for UV spectroscopy ($\lambda = 750$ nm) are presented in Figure 4. The parameters estimated by the model are presented in Table 4. Values of diffusivity and asphaltene aggregate diameter are in agreement with other results reported in the literature.[29] A long duration test (21 days) has also been performed, and the saturation was reached for 3.5 wt % of asphaltene deposited on the solid, which corresponds to a surface coverage of 2.5 mol m^{-2}, which is also in the range of literature data.[28] Assuming a spherical shape of the asphaltene aggregate, this surface coverage is close to 16 wt %. In the standard experimental conditions (17 h), the amount of deposited asphaltene is close to 1 wt %. We will neglect the impact of this low carbonaceous deposit; therefore, textural properties are supposed to be unchanged during the adsorption experiment.

A parameter sensitivity study has been carried out, by calculating the influence of the variation of the estimated parameters on the model output. A parameter θ_j is experimentally identifiable if its sensitivity is not negligible, $S_j = (\partial\phi^f_{asp}(t)/\partial\theta_j) \neq 0$, and if its sensitivity is not proportional to the sensitivity of any other parameter, $S_j = (\partial\phi^f_{asp}(t)/\partial\theta_j) \neq A(\partial\phi^f_{asp}(t)/\partial\theta_k)\ \forall\ k \neq j$, where $\phi^f_{asp}(t)$ is the output of the model, θ_j is the input parameter, and

(39) Couenne, F.; Jallut, C.; Tayakout, M. *Comput. Chem. Eng.* **2005**, *30*, 42–53.
(40) Tayakout, M.; Jolimaître, E.; Jallut, C. *Chem. Eng. Sci.* **2000**, *55*, 2945–2956.
(41) Broekhoff, J. C. P.; de Boer, J. H. *J. Catal.* **1967**, *9*, 8–14.

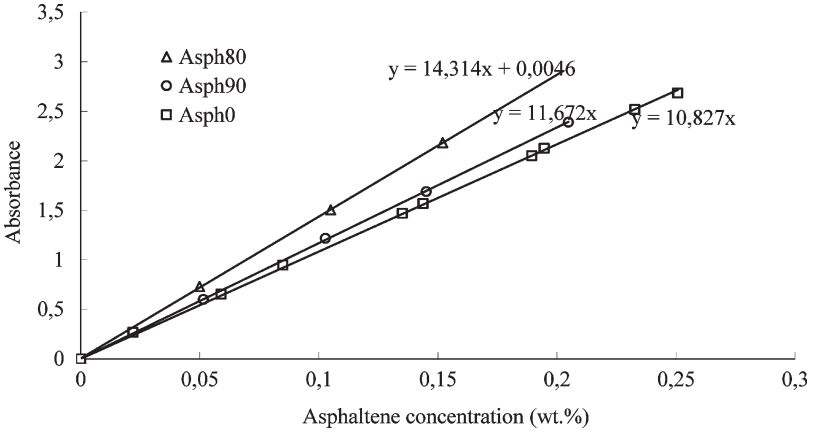

Figure 4. UV spectroscopy calibration curves determined for $\lambda = 750$ nm: (□) unconverted asphaltenes, (△) 80% converted asphaltenes, and (○) 90% converted asphaltenes.

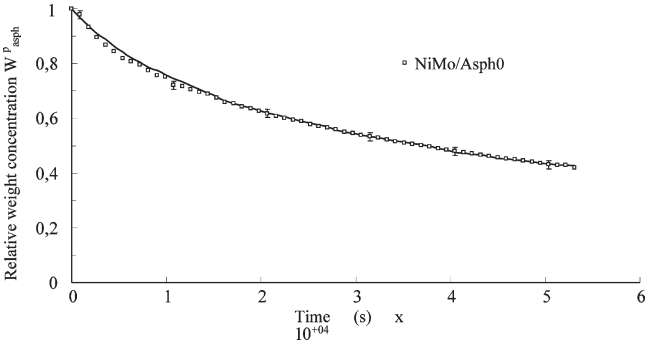

Figure 5. Relative weight concentration of unconverted asphaltene aggregates versus time with reference NiMo catalyst: experimental data (□) and modeling results (—).

Table 4. Adjusted Parameters for the Diffusion of Unconverted Asphaltenes (Asph0) in the Fresh Catalyst (Fresh Cat)

catalyst/asphaltene	fresh cat/Asph0
Estimated Parameters	
D_∞ (m^2/s)	$1.3 \times 10^{-10} \pm 1.4 \times 10^{-11}$
b_{asp} (m^3/mol)	9.1 ± 1.3
q^{max} (mol/m^3)	71 ± 10
b_{tol} (m^3/mol)	$7.8 \times 10^{-6} \pm 8.5 \times 10^{-7}$
$n_{s,asp}$	32 ± 9
Calculated Parameters	
D_{eff} (m^2/s)	7.8×10^{-12}
D_h (Å)	59
M_w (g/mol)	3972

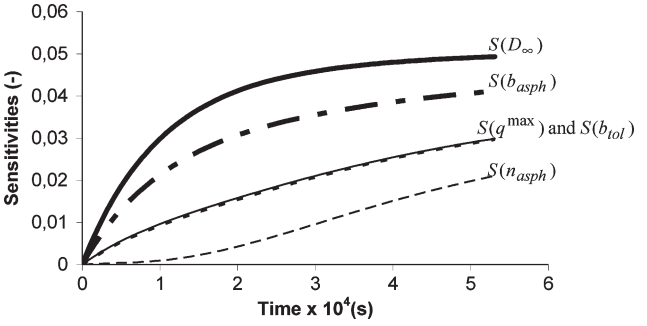

Figure 6. Evolution with time of the normalized sensibilities for the five estimated parameters: the translational diffusion coefficient [$S(D_\infty)$], the toluene thermodynamical parameter [$S(b_{tol})$], the asphaltene thermodynamical parameter [$S(b_{asph})$], the saturation concentration [$S(q^{max})$], and the asphaltene segment number [$S(n_{asph})$].

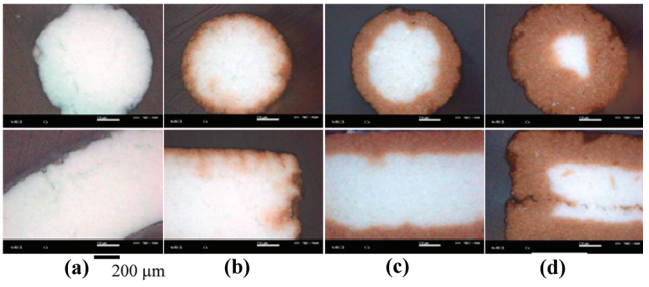

Figure 7. Pictures of radial and longitudinal sections of (a) fresh NiMo/Al_2O_3 extrudates, (b) after 2 h in contact with unconverted asphaltenes, (c) after 17 h, and (d) after 21 days (100× magnification).

A is a constant independent of time. Results are displayed in Figure 6. All of the parameters are sensitive in our experimental conditions; that is to say, no parameter can be neglected *a priori*. The translational diffusion coefficient (D_∞) is the most sensitive, followed by b_{asph} and b_{tol}, q^{max}, and n_{asph}, respectively. Moreover, all of the sensitivities are distinct except for b_{tol} and q^{max}.

The penetration depth of the asphaltene aggregates can also be followed by optical microscopy (Figure 7). After a short contact time (2 h), the solution starts to fill the porous network of the catalyst but still remains mostly located at the outer shell of the extrudate. After 17 h of experiment, almost $^1/_3$ of the extrudate volume is browned by asphaltene solution with a darker coloration than after 2 h. After a much longer period (21 days), the extrudate is not yet completely filled because a white area is still visible. The coloration is quite similar than after 17 h, but the surface occupied by asphaltenes has grown; about 80% of the porous surface is then filled with asphaltenes. These results show that, in these conditions, the diffusion process of the unconverted asphaltene aggregate may go on even after 21 days of exposure. Nevertheless, if one estimates the average penetration depth ($\langle x \rangle$) from the modeling results using the equation ($\langle x \rangle = 2(tD_{eff}/\pi)^{1/2}$), we find a much larger distance for the different durations, circa 4 and 10 times the distance measured according the colored zone on the micrograph for 2 and 17 h, respectively (Figure 7). For instance, a comparable penetration depth with $t = 17$ h (about 0.3 mm) can be obtained if we consider the diffusion of bigger asphaltene aggregates (average size $D_h = 180$ Å), or limit the diffusion of the previous (smaller) asphaltene aggregates ($D_h = 59$ Å) in pores not larger than 70 Å. This discrepancy may be explained by the fact that the previous integrated equation

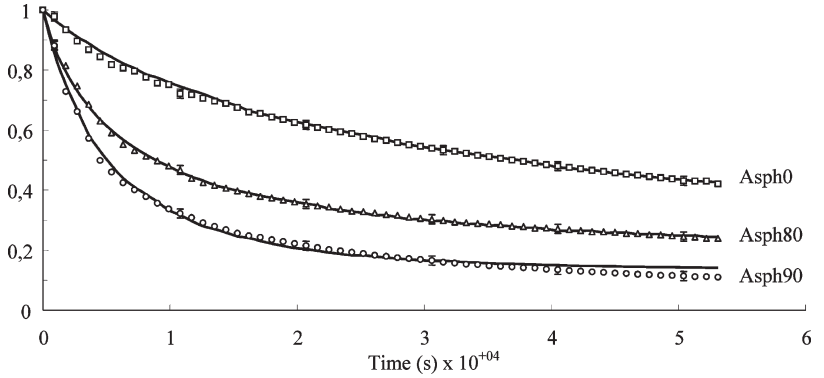

Figure 8. Relative weight concentration of asphaltenes at different conversions versus time with reference (NiMo) fresh catalyst. Comparison between the experimental data (○, △, and □) and modeling results (—).

Table 5. Adjusted Parameters for the Diffusion of Unconverted Asphaltenes (Asph0) and Converted Asphaltenes (Asph80 and Asph90) in the Fresh Catalyst

catalyst/asphaltene	fresh cat/Asph0	fresh cat/Asph80	fresh cat/Asph90
		Estimated Parameters	
D_∞ (m^2/s)	$1.3 \times 10^{-10} \pm 1.4 \times 10^{-11}$	$3.8 \times 10^{-10} \pm 5.5 \times 10^{-11}$	$4.2 \times 10^{-10} \pm 2.2 \times 10^{-11}$
b_{asp} (m^3/mol)	9.1 ± 1.3	13.2 ± 2.3	15.9 ± 1.2
q^{max} (mol/m^3)	71 ± 10	70 ± 11	68 ± 10
b_{tol} (m^3/mol)		$7.8 \times 10^{-6} \pm 8.5 \times 10^{-7}$	
$n_{s,asp}$	32 ± 9	17 ± 3	14 ± 2
		Calculated Parameters	
D_{eff} (m^2/g)	7.8×10^{-12}	5.5×10^{-11}	6.2×10^{-11}
D_h (Å)	59	19	18
M_w (g/mol)	3972	2075	1680

overestimates the penetration depth for a given duration. Indeed, it does not consider the decrease over time of the D_{eff} coefficient because of the pore plugging as a result of the continuous asphaltene deposition (decrease of ε_p, intragranular porosity, and d_o, average pore diameter). This is also consistent with the fact that this disparity increases with time.

Effect of the Asphaltene Conversion Level. Figure 8 shows the variation of the relative weight concentration versus the hydroconversion level of the asphaltenes. Results of modeling are presented in Table 5. The effective diffusion coefficient D_{eff} is increased by a factor of 8 from the unconverted to the 90% converted asphaltene aggregates when, at the same time, the adsorption constant is also increased (from 9.1 to 15.9). The size of the residual asphaltene aggregates at high conversion is about a third of the ones of the feed, with no significant difference between 80 and 90% conversion. The average number of the segment ($n_{s,asph}$) decreases when conversion increases, indicating the variation of the molar volume of the asphaltene aggregates. This variation is likely to be due to the structural modifications during hydroconversion under severe operating conditions. Indeed, it is reported in the literature that, above 50% of conversion, the chemical structure of asphaltene units still significantly evolves through dealkylation mechanisms, leading to highly peri-condensed structures, which survive at higher conversion levels.[26] These residual structures exhibit high aromaticity and polarity and less steric hindrance for adsorption and, as a consequence, may develop stronger interactions with the alumina surface sites.

Pictures of the extrudates after 17 h of experiments clearly illustrate the penetration profiles into the catalyst grains for the different types of asphaltene aggregates (Figure 9). Whereas a core shell repartition is observed in the case of the unconverted structures, penetration is much more pronounced and the repartition more homogeneous when the asphaltene aggregates are converted in agreement with the previous results.

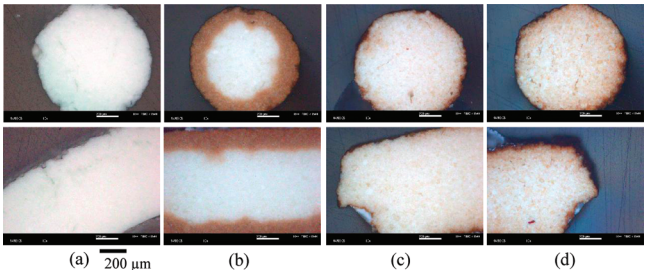

Figure 9. Pictures of radial (top panels) and longitudinal (bottom panels) sections of (a) fresh $NiMo/Al_2O_3$ extrudates and after 17 h in contact with (b) Asph0, (c) Asph80, and (d) Asph90.

Diffusion−Adsorption on Spent NiMo Catalyst. Figure 10 shows the effect of the coke deposit during the hydroconversion of the vacuum residue on the kinetics of diffusion−adsorption in the case of unconverted asphaltene structures. The parameters obtained from the model are listed in Table 6. Data show that the adsorption constant (b_{asph}) and saturation concentration (q^{max}) are markedly affected by the coke deposition. Coke deposition increases hydrophobicity of the surface and neutralizes acidic sites, which are supposed to act as adsorption sites for asphaltenes via basic nitrogen.[15,16,42] In the same time, textural properties are modified by coke deposition; the mesoporous volume (pores size between 70 and 500 Å, where resistance transfer occurs) is divided by

(42) Bartholomew, C. H. *Appl. Catal., A* **2001**, *212*, 17–60.

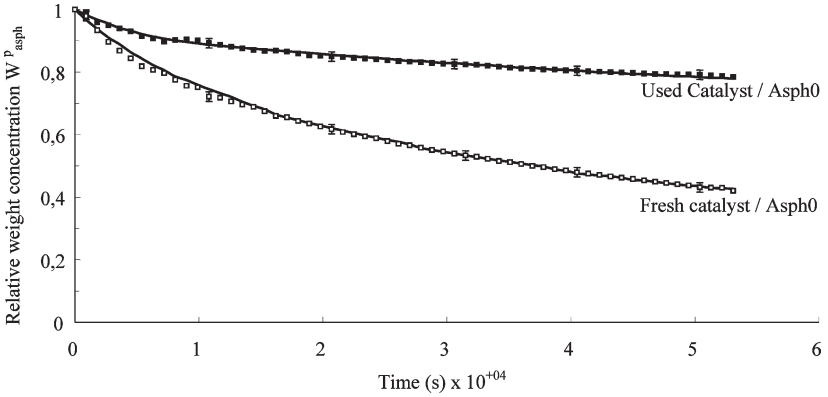

Figure 10. Relative weight concentrations of Asph0 versus time for the fresh and used catalysts: experimental data (□ and ■) and modeling results (—).

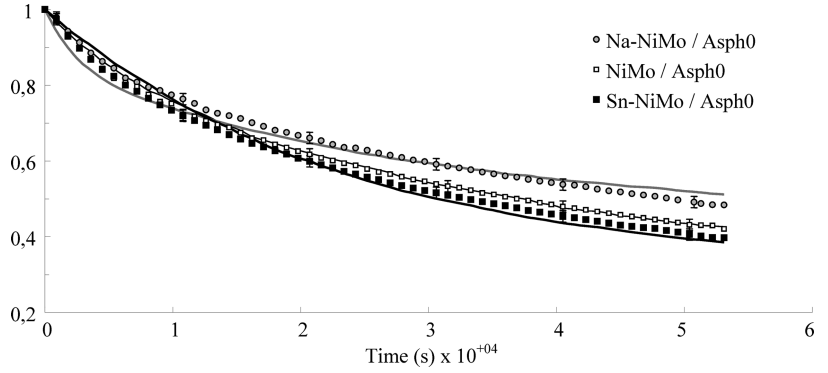

Figure 11. Relative weight concentration of asphaltenes versus time for unconverted asphaltenes (Asph0) for the fresh catalyst and sodium- and tin-doped ones: (■, □, and gray ○) experimental data and (—) modeling results.

Table 6. Adjusted Parameters for the Diffusion of Unconverted Asphaltenes (Asph0) on the Fresh (Fresh Cat) and Used (Used Cat) Catalyst

catalyst/ asphaltene	fresh cat/ Asph0	used cat/ Asph0
	Estimated Parameters	
D_∞ (m^2/s)	$1.3 \times 10^{-10} \pm 1.4 \times 10^{-11}$	
b_{asp} (m^3/mol)	9.1 ± 1.3	4.2 ± 0.4
q^{max} (mol/m^3)	71 ± 10	31 ± 5
b_{tol} (m^3/mol)	$7.8 \times 10^{-6} \pm 8.5 \times 10^{-7}$	$5.2 \times 10^{-6} \pm 6.0 \times 10^{-7}$
$n_{s,asp}$	32 ± 3	
	Calculated Parameters	
D_{eff} (m^2/g)	7.8×10^{-12}	4.1×10^{-12}
D_h (Å)	59	
M_w (g/mol)	3972	

a factor of 2 by coking. This has a direct impact on the intragranular porosity ε_p, which decreases from 0.202 to 0.101 (Table 2), and as a consequence, effective diffusivity is strongly decreased by coke deposition, as shown in Table 6.

Effect of the Modification of Acidobasic Surface Properties by the Addition of Dopants. Figure 11 shows the variation of the relative weight concentration versus time for the experiments carried out with the unconverted asphaltene units on the different modified catalysts. The adjusted and calculated parameters are presented in Table 7. The differences are rather small but significant, and the final asphaltene concentration for the solution catalyst is higher for Na−NiMo than for NiMo (reference) and Sn−NiMo catalysts; the consumption of asphaltenes is the slightly faster in this last case. We can notice that the only parameter that is modified is the asphaltene adsorption constant (b_{asph}), which increases in the case of the Sn-modified catalyst and slightly decreases in the case of Na doping, compared to the starting NiMo solid. Because textural properties of the support are not modified by the impregnation of the dopants as checked by N_2 isotherms, no change in the diffusion coefficients is expected as confirmed by the calculation. These tendencies are in agreement with an adsorption process involving acidic centers of the alumina, which are inhibited by Na deposition.[19] Tin doping is also expected to decrease alumina acidity[43,44] but to a much lesser extent, and as a compensation effect, SnO_x clusters may also act as new adsorption sites for asphaltene molecules.

Figure 12 shows the case of highly converted asphaltene structures (Asph90) used in the same conditions for the different modified catalysts. As already observed for the dopant-free catalyst, the concentration decrease in the solution is drastically faster than in the case of unconverted aggregates, but no significant differences can be observed anymore between the different catalysts. Converted asphaltene dynamic of diffusion−adsorption is no longer modified by the presence of the dopants and the associated surface property modifications. The values of the fitted parameters (not presented here) are the same as the reference catalyst within accuracy. The structure of the aggregates seems to play a role because the residual asphaltenes of hydroconversion performed at high temperature are known to have a high degree of condensation (aromaticity) and

(43) Sheng, T. C.; Kirszensztejn, P.; Bell, T. N.; Gay, I. D. *Catal. Lett.* **1994**, *23*, 119–126.
(44) Sprinceana, D.; Caldararu, M.; Ionescu, N. I.; Auroux, A. *J. Therm. Anal. Calorim.* **1999**, *56*, 109–115.

Table 7. Adjusted Parameters for the Diffusion of Unconverted Asphaltenes (Asph0) in the Doped Catalysts

catalyst/asphaltene	NiMo/Asph0	Na−NiMo/Asph0	Sn−NiMo/Asph0
		Estimated Parameters	
D_∞ (m^2/s)		$1.3 \times 10^{-10} \pm 1.4 \times 10^{-11}$	
b_{asp} (m^3/mol)	9.1 ± 1.3	7.3 ± 1.3	10.6 ± 1.1
q^{max} (mol/m^3)	71 ± 10	71 ± 9	71 ± 10
b_{tol} (m^3/mol)	$7.8 \times 10^{-6} \pm 8.5 \times 10^{-7}$	$7.8 \times 10^{-6} \pm 4.1 \times 10^{-7}$	$7.8 \times 10^{-6} \pm 5.5 \times 10^{-7}$
$n_{s,asp}$		32 ± 9	
		Calculated Parameters	
D_{eff} (m^2/g)	7.8×10^{-12}	7.7×10^{-12}	8.2×10^{-12}
D_h (Å)		59	
M_w (g/mol)		3972	

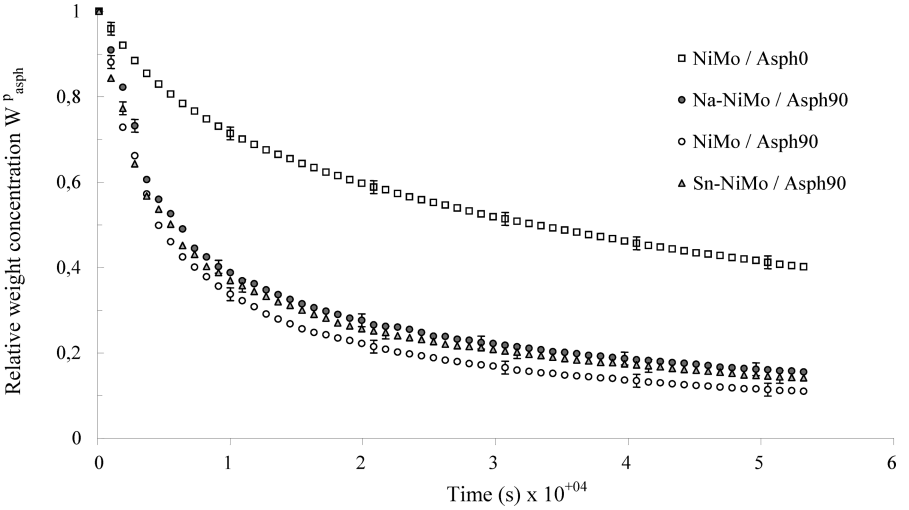

Figure 12. Relative weight concentration of asphaltenes versus time, for unconverted (Asph0) and converted (Asph90) with reference (NiMo) and converted (Asph90) with Na−NiMo and Sn−NiMo.

a lower solubility, compared to the asphaltenes present in the initial feedstock.[26]

Conclusion

The influence of different parameters, such as the conversion level of asphaltenes after the hydroconversion test, coke deposition, and acidobasic properties of a $NiMo/Al_2O_3$ catalyst on the diffusion−adsorption process, have been investigated by UV spectroscopy. A modeling approach based on Stefan−Maxwell equations adapted to volume constraints has been applied to extract separately diffusion and adsorption parameters. Diffusion of deeply converted asphaltene structures is strongly enhanced as their size decreases, while the adsorption coefficient increases in agreement with the higher aromaticity of residual asphaltene units, which are able to interact more strongly with the surface sites of the catalyst. The coke deposit on the catalyst during the hydroconversion test decreases both the adsorption constant by a passivation effect of the acidic surface sites and diffusion coefficient by plugging the porosity of the catalyst. Finally, modification of the acidobasic properties of surface sites, by sodium or tin addition, plays a minor role in our conditions compared to the previous parameters, even if one can notice a slight decrease of the adsorption constant with Na addition and an opposite tendency in the case of Sn doping when unconverted asphaltenes are considered.

Acknowledgment. The authors thank David Goncalves, Hélène Biguerd, and Didier Espinat for UV spectroscopy measurements and fruitful discussions.

Nomenclature

A = absorbance
Asph0 = unconverted asphaltene aggregates
Asph80 = asphaltene aggregates converted at 80 wt %
Asph90 = asphaltene aggregates converted at 90 wt %
b_i = thermodynamic Langmuir coefficient of component i (m^3/mol)
c = concentration of asphaltenes in the solution (mol/m^3)
C_i^p = concentration of component i inside the porous phase (mol/m^3)
C_i^f = concentration of component i in the fluid phase (mol/m^3)
C_T = total concentration (mol/m^3)
D_{eff} = effective diffusion coefficient (m^2/s)
D_g = giration diameter (m)
D_h = hydrodynamic diameter or diameter of a given molecule considered as a sphere (m)
d_o = average pore diameter (m)
D_∞ = bulk phase diffusion coefficient or translational diffusion coefficient (m^2/s)
D_{ij} = Stefan−Maxwell binary diffusion coefficient (m^2/s)
I = intensity of the monochromatic radiation
I_o = intensity of the incident radiation
I_{ref} = intensity of the radiation of the reference cell
k = Boltzmann constant (J/K)
k_i = mass-transfer coefficient of component i corresponding to the fluid phase (m/s)
K_p = partition of the solute coefficient
K_r = coefficient that considers the viscous drag of the molecule

l = cell thickness (m)
M_w = molar weight (kg/mol)
n_c = number of components
$n_{s,i}$ = number of segments of component i, compared to the elementary volume
q_{max} = saturation concentration (mol/m^3 of solid)
q_i = concentration of component i in the adsorbed phase (mol/m^3 of solid)
R = ideal gas constant (J mol^{-1} K^{-1})
R_h = hydrodynamic radius or radius of a given molecule considered as a sphere (m)
R_p = pellet radius (m)
r_o = pore radius (m)
$S(D_\infty)$ = sensitivity of the translational diffusion coefficient, $S(D_\infty) = (\partial\phi^f_{asp}(t)/\partial D_\infty)$
$S(b_i)$ = thermodynamic Langmuir coefficient sensitivity of component i, $S(b_i) = (\partial\phi^f_{asp}(t)/\partial b_i)$
$S(q^{max})$ = sensitivity of the saturation concentration, $S(q^{max}) = (\partial\phi^f_{asph}(t)/\partial q^{max})$
$S(n_{s,asph})$ = sensitivity of the translational diffusion coefficient, $S(n_{s,asph}) = (\partial\phi^f_{asp}(t)/\partial n_{s,asph})$
Sc = Schmidt number, $(\eta_i/\rho_T D_{ij})$
SVR = Safaniya vacuum residue
T = temperature (K)
V_c = crystal volume (m^3)
V_{meso} = mesoporous volume by catalyst mass (mL/g)
V_{macro} = macroporous volume by catalyst mass (mL/g)
$V(r,t)$ = porous volume, for pores of radius r and time t
W_i^p = mass fraction of component i in the porous phase
$W_i^{0,p}$ = initial mass fraction of component i in the porous phase
$W_i^{0,f}$ = mass fraction of component i in the fluid phase

Greek Symbols

ϑ^0 = molar volume of the elementary segment (m^3/mol)
ϑ_i = molar volume of component i (m^3/mol)
ε = molar absorption coefficient (L mol^{-1} cm^{-1})
ε_i = extragranular porosity
ε_p = intragranular porosity
λ = ratio between the molecule and pore radius
ϕ_i^p = volume fraction of component i adsorbed on solid
ϕ_i^f = volume fraction of component i in the extragranular fluid phase
ρ_i = density of component i (kg/m^3)
η_i = viscosity of component i (Pa s)
μ_i = chemical potential of component i

Subscripts

asph = asphaltene
tol = toluene